Lateral Forces in Rolling-Cut Shearing and Their Consequences on Common Edge Defects

Alexander Zeiler[1]
Automation and Control Institute (ACIN),
TU Wien,
Vienna, Austria
e-mail: zeiler@acin.tuwien.ac.at

Andreas Steinboeck
Automation and Control Institute (ACIN),
TU Wien,
Vienna, Austria
e-mail: steinboeck@acin.tuwien.ac.at

Andreas Kugi
Automation and Control Institute (ACIN),
TU Wien,
Vienna, Austria
e-mail: kugi@acin.tuwien.ac.at

Martin Jochum
AG der Dillinger Hüttenwerke,
Dillingen, Germany
e-mail: martin.jochum@dillinger.biz

Lateral Forces in Rolling-Cut Shearing and Their Consequences on Common Edge Defects

This paper deals with the detailed analysis of the lateral process forces in rolling-cut shearing of heavy steel plates and their impact on edge defects. Rolling-cut shearing is still the most common method of heavy-plate side trimming. However, this method can entail edge defects like uneven longitudinal shape as well as burr and fractures in the area of the cut-changeover (beginning and end of the periodical cuts). In the existing literature, neither the root cause of these edge defects nor their nexus with the upper blade trajectory (blade drive-kinematics) has been analyzed in detail. In this work, these issues will be explored based on the finite element method (FEM) simulations and measurements from an industrial plant. The complex interrelation between drive-kinematics, varying lateral force, unintended lateral motion of the upper blade, unintended variation of the blade clearance, and quality defects is analyzed. The variation of the lateral force is identified as the root cause of such quality defects and a physical explanation for variations of the lateral force is given. The detailed understanding of the shearing process serves as a solid basis for an optimization and re-design of the drive-kinematics in a future work. Measurements from an industrial plant and simulation results show good agreement and thus confirm the theory. The results are transferable to other rolling-cut trimming shears.
[DOI: 10.1115/1.4042578]

1 Introduction

Side trimming is an essential processing step in the finishing line of heavy-plate rolling plants. From an economic point of view, time-efficient trimming of large quantities of plates is necessary. The most common method of heavy-plate side trimming is mechanical shearing [1]. Side trimming by flame cutting is an alternative technology but achieves only significantly slower process speed and the area around the edge is exposed to high thermal stresses. However, mechanical shearing of heavy plates can cause shape defects of the edges. In both cases, cost-intensive post-processing steps like edge grinding are required. Therefore, there is a high economic demand to ensure both time-efficiency and high-quality sheared edges.

The contemporary technique for side trimming of heavy plates is periodic double-sided rolling-cut shearing. For heavy plates, the trimming procedure is usually carried out as a cold forming process. This type of shear consists of a fixed, straight lower blade and an arc-shaped (typically circular), moveable upper blade on each side. The upper blade performs a fixed periodic motion in the yz-plane (see Fig. 1), which is governed by a seven-bar linkage, consisting of connecting rods, crankshafts, eccentric bolts, and the blade carriage. The authors of Ref. [2] released a detailed description of a comparable seven-bar linkage. These linkages are typically driven by electrical machines with constant rotational speed (often stabilized by flywheels). The upper blade is backlash-free guided by wearing plates, which should ensure a pure motion in the yz-plane.

In the first step (Fig. 1(a)), the upper blade separates the so-called scrap (orange) from the usable plate area (purple) by a rolling-cut . Simultaneous to this longitudinal separation, the scrap from previous cuts is transversally split up by a scrap knife (Fig. 1(b)). An additional top view of the mechanism is shown in Fig. 2. In the second step, when there is no more contact between the upper blade and the plate, two pairs of pinch rolls move the whole plate with an adjustable feed rate (Fig. 1(c)). After the transport of the plate, the trimming process restarts at the first step. A vital quantity in nonparallel-blade shearing is the shearing angle α_s. In rolling-cut shearing, α_s is defined as the angle between the straight lower blade and the tangent line of the upper blade at the shearing point $\boldsymbol{p}_s = [y_s\ z_s]^\mathrm{T}$ (see Fig. 1(a)). This is the point where the material fracture currently occurs (see Fig. 2). The first component of the vector $\boldsymbol{p}_s$ calculates to $y_s = (1-\varepsilon_s)t_p$, where the parameter ε_s denotes the vertical penetration of the upper blade until fracture occurs and t_p is the plate thickness. Because the parameter ε_s can be easily determined by visual inspection, the shearing angle $\alpha_s(t)$ and the point of material fracture $z_s(t)$ on the z-axis can be calculated based on the drive-kinematics and the plate thickness.

The design of rolling-cut shears aims at imitating the well-proved full-circle disc trimming shears. This type of shear consists of a full-circle disc blade, which performs a pure rotational motion. Pinch rolls move the plates with a constant speed in order to straightly trim their side edges. With this type of shears, good-quality edges and fast processing speed are achieved for plates up to 25 mm thickness [3]. However, to ensure a desirable shearing angle α_s of 1 deg to 4 deg for thicker plates [4], an enormous and practically not feasible diameter of the full-circle disc would be necessary. Therefore, the seven-bar drive-kinematics was introduced to reproduce the pure-rolling motion of full-circle disc trimming shears as accurately as possible. However, the impact of deviations between the ideal pure rolling motion and the motion realized by the seven-bar linkage has not yet been investigated in detail in the literature. An analysis of this impact is thus one of the main objectives of the present work.

Rolling-cut shears can lead to quality defects like burr, fractured areas, and rollover, which are well known from related shearing methods like blanking. In Ref. [5], the optimal horizontal clearance between upper and lower blade is worked out in order to minimize the mentioned defects. The influence of the clearance on the edge quality was investigated by Murakawa and Lu [4].

[1]Corresponding author.
Manuscript received March 26, 2018; final manuscript received December 11, 2018; published online February 27, 2019. Assoc. Editor: Yannis Korkolis.

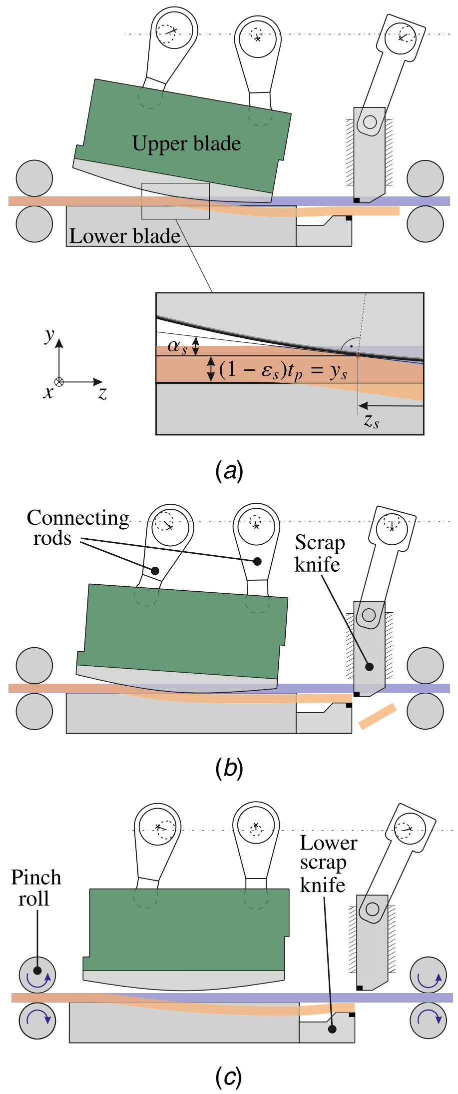

Fig. 1 The rolling-cut principle

An uneven shape of the sheared edge in the longitudinal direction is a crucial quality defect in rolling-cut shearing (RCS). This defect often materializes in the form of sawtooth-shaped edges (Fig. 3). Thus, a local deviation from the target plate width and contour shape occurs. In particular, the edge quality in the region of the cut-changeover (end of the previous cut and beginning of the following cut) can be poor (discontinuity of the edge). Figure 4(*a*) shows a typical poor-quality edge around the cut-changeover. A proper edge section in the nonchangeover area is shown in Fig. 4(*b*). In Ref. [6], a similar phenomenon is observed. The authors of

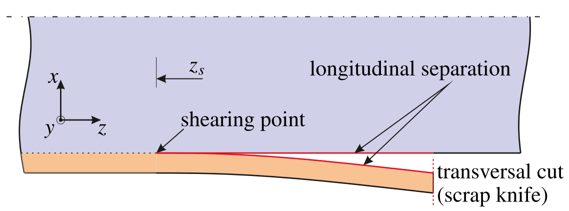

Fig. 2 The rolling-cut principle (top view)

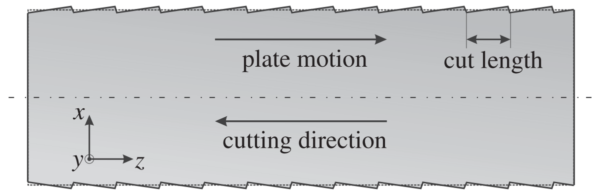

Fig. 3 Typical longitudinal shape of the sheared edge

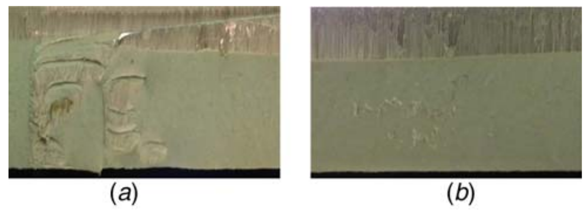

Fig. 4 (*a*) Comparison of edge section around the cut-changeover and (*b*) in-between the changeovers

Ref. [7] found that fluctuations of the clearance within a single cut can result in defects such as local fractures and locally amplified burr. The negative impact of a varying clearance within a cut is also well known from blanking as it is described in the PhD thesis of Nothhaft [8]. She investigated the varying clearance due to lateral forces in shearing with parallel blades. In this case, varying clearance limits the edge quality and increases the tool wear. In parallel blade shearing, a change of the clearance has almost no impact on the longitudinal shape of the edge. In rolling-cut shearing, however, this impact is significant.

In view of the typical edge defects that can occur in RCS, there is a lack of publications on the nexus between varying clearance, blade geometry and motion, and lateral forces in RCS. The roots, magnitude, and consequences of lateral forces in RCS are still widely unknown. This is the main motivation for studying the following causal chain in the present paper: suboptimal blade geometry and drive-kinematics → varying lateral force → unintended lateral motion of the upper blade (i.e., unintended variation of clearance) → quality defects at the edge. A physical explanation for the variation of the lateral forces in RCS will be given in this paper. Furthermore, the dependence of the lateral force on the typical blade-kinematics of rolling-cut shears will be analyzed. In this context, RCS will also be compared with full-circle disc trimming shears.

For a deeper understanding of the process and to identify the essential reasons for edge defects in RCS (especially at the cut-changeover), 3D-FEM simulations and measurements of the lateral upper blade motion in an industrial rolling-cut shear will be used. The measurements also serve as a basis for the validation of the FEM model. The authors of Ref. [1] also presented a 3D-FEM simulation of the rolling-cut process. However, they mainly focus on simulation-specific aspects. The process itself is not analyzed in detail [1]. Another 3D-FEM simulation of a drilling process is described in Ref. [9]. In this work, insights into the usage of a suitable material and damage models are given. Additionally, they investigated the formation of burr based on the conducted simulations and experiments.

An in-depth understanding of the physical effects that cause the lateral forces and their relation to the drive-kinematics allows a more suitable design of the drive-kinematics of rolling-cut shears. An improved design would presumably ensure constant lateral forces and consequently constant clearance. Thus, defects at the cut-changeover could be avoided or highly reduced. Additionally, a constant clearance at any point $z_s(t)$ in between the cut-changeover area would lead to equal fracture behavior over the entire edge.

This paper is organized as follows: In Sec. 2, an FEM simulation of the RCS process is presented. Experimental setups for measuring

Post-print version of the article: A. Zeiler, A. Steinboeck, A. Kugi, and M. Jochum, “Lateral forces in rolling-cut shearing and their consequences on common edge defects,” *Journal of Manufacturing Science and Engineering*, vol. 141, no. 4, 41001-1–41001-9, 2019. DOI: 10.1115/1.4042578
The content of this post-print version is identical to the published paper but without the publisher’s final layout or copy editing.

the lateral motion of the upper blade and the longitudinal edge shape are described in Secs. 3 and 4, respectively. Simulation and measurement results are presented and compared in Sec. 5. The physical causes of the lateral force and the dependence on the blade drive-kinematics are discussed in Sec. 6. Section 7 contains a brief summary and an outlook on future research possibilities.

2 FEM Simulation of the Rolling-Cut Process

The main objectives of the FEM simulation are to compute the forces acting on the blades during the rolling-cut process and to study the influence of the drive-kinematics. Special attention is given to the forces and the displacements of the upper blade along the x-direction. The FEM simulation is done for an industrial rolling-cut shear used in the rolling mill plant of AG der Dillinger Hüttenwerke (Dillingen/Saar, Germany).

2.1 Simulation Setup and Assumptions. The commercial code ABAQUS/Explicit is used for the numerical simulations. This software is well suited for large deformations and nonlinear contact problems [10]. The analysis is carried out with 3D geometry to investigate the influence of both drive-kinematics and blade geometry. Due to symmetry reasons, only one side of the trimming process is considered, see Fig. 5. An interaction between the trimming sides is not expected, because the plate is assumed to be fixed by blank holders. The circular upper blade is equipped with a radius of 9.8 m and has a length of 2.08 m. These values are chosen based on the industrial rolling-cut shear. The blades and the scrap knife are modeled as rigid shells and consist of elements of the type R3D4 and R3D3. For the bottom blades, these elements are totally constrained. For the upper blade, it strictly performs the pre-calculated rolling motion defined by the drive-kinematics. A derivation of the equations of motion for a seven-bar linkage can be found in Ref. [2]. In Sec. 2.3, the model will be enhanced by boundary conditions that emulate the lateral compliance of the upper blade. The considered plate has a thickness of 30 mm and its material is steel grade AISI 1045. The material properties and the applied constitutive material model are discussed in Sec. 2.2. To minimize the computational effort, just a part of the plate relevant for the considered cut is modeled. This part includes the scrap from the previous cut (see Fig. 2), which lies on the lower scrap knife at its end (see Fig. 5). As will be discussed in Sec. 6, the curvature of the scrap, which is constrained by the lower scrap knife, influences the lateral forces on the upper blade. The plate is discretized using 3D hexahedral elements (C3D8R), with a minimum mesh size of 1 mm × 1 mm × 1 mm in the area around the material fracture. In the transition regions between different mesh sizes, tetrahedral elements (C3D4) are used.

Summarizing, the following assumptions are made:

- The upper blade, the lower blade, and the scrap knife exhibit very small deformation during shearing. This assumption may be inferred from Ref. [1], where the slitting of thick steel plates is studied.
- The plate is ideally clamped by the blank holder. The blank holder is modeled as a fixed geometric boundary condition of the plate.
- Tool wear does not occur. The cutting edges of the blades have an ideal rectangular shape. In Ref. [11] it has been observed that in practical experiments tool wear has only an insignificant impact on the process forces in shearing of heavy plates. Hence, neglecting tool wear is justified when investigating the process forces.
- There is no interaction between the two trimming sides. This is justified because of the assumed ideal clamping by the blank holders.
- The plate material is homogeneous and isotropic (see Sec. 2.2).
- At the blade–plate contact interfaces, Coulomb friction is dominant. For that reason, a Coulomb friction model is used with a friction coefficient of $\mu = 0.2$. The choice of this friction coefficient is based on Ref. [12], where the friction behavior of dry steel sheets was investigated.

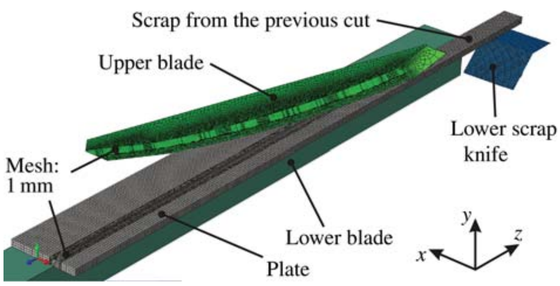

Fig. 5 Meshed FEM model

To overcome excessive element distortion in the region around the material fracture (in further work termed as shear zone), adaptive re-meshing by the arbitrary Lagrangian–Eulerian method is performed. Excessive element distortion could lead to improperly reproduced contact conditions, loss of element accuracy, and therefore unacceptable model inaccuracies [13]. The mass scaling procedure is applied to the region with fine mesh resolution around the material fracture. This enhances the computational efficiency. Convergence studies were conducted to ensure proper mesh sizes, mass scaling, and re-meshing.

2.2 Constitutive and Damage Model for the Plate Material. Steel grade AISI 1045 is commonly used in heavy-plate rolling. This plate material tends to pronounced sawtooth shaped edges when trimmed (Fig. 3). Hence, this material is a good choice for studying edge defects in RCS. Relevant material parameters are summarized in Table 1.

The elastic behavior is assumed to be linear and the plastic behavior is modeled by the isotropic hardening law

$$\sigma_y = \sigma_y^0 + k_p (\bar{\varepsilon}^p)^n \tag{1}$$

Here, $\bar{\varepsilon}^p$ denotes the plastic equivalent strain and σ_y is the yield stress. The influence of the strain-rate is neglected, because the process is assumed to be quasi-static. The damage and failure behavior are described by the Johnson and Cook failure model [15]. The damage initiation criterion is based on the plastic equivalent strain $\bar{\varepsilon}^p$ at each element integration point and is given by

$$1 \le \frac{\bar{\varepsilon}^p}{\bar{\varepsilon}^p_D(\eta)} \tag{2}$$

where $\bar{\varepsilon}^p_D(\eta)$ is the strain at damage initiation. As newer studies like Ref. [16] confirm, $\bar{\varepsilon}^p_D$ strongly depends on stress triaxiality η. The triaxiality is defined as

$$\eta = \frac{\sigma_v}{\sigma_h} \tag{3}$$

where σ_v is the von Mises equivalent stress and σ_h the hydrostatic stress. The triaxiality indicates the type of load (i.e., tensile-,

Table 1 Mechanical properties of the steel grade AISI 1045 [14]

Parameter	Symbol	Value
Young's modulus	E	205 GPa
Poisson's ratio	ν	0.29
Initial yield strength	σ_y^0	615 MPa
Material constant	k_p	667 MPa
Strain hardening exponent	n	0.255

Post-print version of the article: A. Zeiler, A. Steinboeck, A. Kugi, and M. Jochum, "Lateral forces in rolling-cut shearing and their consequences on common edge defects," *Journal of Manufacturing Science and Engineering*, vol. 141, no. 4, 41001-1–41001-9, 2019. doi: 10.1115/1.4042578
The content of this post-print version is identical to the published paper but without the publisher's final layout or copy editing.

compressive-, or shear loading) an infinitesimal element is exposed to. The implemented formulation of the Johnson and Cook criterion defines the plastic equivalent strain at damage initiation as

$$\bar{\varepsilon}_D^p(\eta) = \left(d_1 + d_2 \exp(-d_3\eta)\right) \tag{4}$$

Here, d_1, d_2, and d_3 are material-dependent failure parameters that have to be identified based on experiments. Similar to the plasticity formulation given in Eq. (1), the influence of the strain rate is neglected in Eq. (4). Once the initiation criterion (2) is met for an integration point, the material stiffness for this element is degraded linearly with $\bar{\varepsilon}^p$ until the element lost its load-carrying capacity. Then, this element gets removed from the mesh (the element-kill method).

The authors of Ref. [14] performed a parameter identification of the Johnson and Cook failure parameters for steel grade AISI 1045. The identified values $d_1 = 0.04$, $d_2 = 1.03$, and $d_3 = 1.39$ are also used for the simulations in this paper. Wang's identification is based on multiple experiments, including tensile tests at low triaxiality values, which typically occur in the shear zone [17].

2.3 Simulation of the Lateral Blade Motion. If the upper blade, its drive-kinematics, and its guides are assumed to have zero compliance, the model is suitable for evaluating lateral forces. However, if the lateral motion of the upper blade should also be investigated, a nonzero compliance of the guides of the upper blade must be implemented in the model. In this work, this compliance is modeled by a translational and rotational virtual equivalent spring. This allows the direct comparison of simulation results and motion measurement (see Sec. 3).

At the considered rolling-cut shear, the upper blade is backlash-free plainly guided by two wearing plates (see Fig. 6). These wearing plates are mounted by two horizontal connecting posts, which are linked over a system of rods and eccentric bolts to the ground. The translational equivalent stiffness c_{tr} of this system is approximatively calculated by assuming the involved parts to be linear elastic. This gives $c_{tr} = 450\ \mathrm{Mn\ m^{-1}}$. Because the lateral process force on the upper blade acts at different coordinates z during a single cut, the lateral translational motion of the blade is superimposed by a small but non-negligible rotation. Motion measurements confirm this assertion. The rotational equivalent spring stiffness $c_{tor} = 300$ Mn m rad was identified based on measurements.

Results and a validation of the developed FEM model will be presented in Sec. 5.

3 Measurement of the Lateral Blade Motion

Knowledge of the lateral motion of the upper blade helps to validate the simulation model and gives a deeper understanding of the RCS process. This is why a laser-tracker based 3D position measurement system was temporarily used at the upper blade of the considered industrial rolling-cut shear. This system achieves a nominal accuracy of 0.01 mm at a sampling rate of 100 Hz. For the measurement, two laser reflectors were attached to the side surface of the upper blade along the z-coordinate. One reflector at the beginning and the other one at the end of the upper blade. This configuration allows to measure both a translational motion of the blade in the x-direction and a possible rotation around the y-axis. The trimming process of a 30.9 mm thick plate, including the no-load periods before and after the plate, was recorded. The plate material is very similar to steel grade AISI 1045, for which the required material and damage model parameters are known (see Table 1).

The measurement results are discussed in Sec. 5.

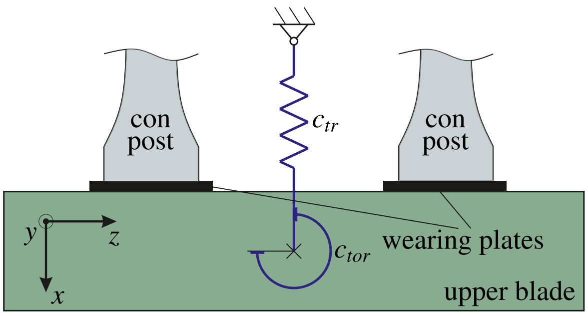

Fig. 6 Schematic illustration of the lateral guiding of the upper blade and the equivalent springs (top view)

4 Measurement of the Longitudinal Edge Shape

For the same plate that was used during the measurements of the motion of the upper blade, the longitudinal edge shape was manually measured after the RCS process. Clearly, the idea here is to study the interrelation between the lateral blade motion and the sawtooth-shaped edge (see Fig. 3). The edge shape $x(z)$ was manually measured at equidistant points along the z-direction with a step size of 50 mm. At each measurement point, the lateral distance between a fixed reference ruler and the side edge of the plate was determined by a taper gauge. The measurement resolution is 0.1 mm, which is sufficient for the considered purpose. The measured edge shape and the measured lateral motion of the blade are compared and discussed in the following section.

5 Results and Model Validation

In this section, at first, the lateral blade motion is investigated using both the FEM simulations and the laser-tracker measurements from the industrial plant. This facilitates a comparison of the results and a validation of the FEM model. In the second step, a clear correlation between lateral upper blade motion and sawtooth edge shape is observed. The third part of this section is dedicated to the lateral process forces, which are the main cause for the lateral blade motion. The origin of the lateral forces and the influence of the drive-kinematics will be discussed in Sec. 6.

Because the lateral forces on the upper blade can also cause a small rotation of the blade with respect to the y-axis, the lateral displacement $u_x(t, z)$ of the blade depends also on the position coordinate z. The displacement that is of interest for the RCS process is the lateral displacement $u_x(t, z_s)$ at the fracture initiation point $z_s(t)$ (shearing point with respect to the z-coordinate). Henceforth, the abbreviation $u_{x,t} = u_x(t, z_s)$ will be used. The trajectory $z_s(t)$ depends on the drive-kinematics and the plate thickness (see Fig. 1(*a*)) and can be calculated in advance.

5.1 Lateral Motion. Figure 7 shows the measured and simulated lateral displacement $u_{x,t}$ of the blade at the shearing point during both the cut and the no-load period. For the measurement during the no-load period (no plate is trimmed), the displacement is shown at the same pre-calculated shearing point $z_s(t)$. The measurement and simulation setups described in Secs. 2.3 and 3 are used. The black dashed lines mark the start and end of the rolling-cut. Positive values of $u_{x,t}$ characterize a blade displacement towards the center of the plate. The measured and simulated displacements $u_{x,t}$ show a good agreement. Compared with the maximum amplitude of $u_{x,t}$, the simulation error is rather small. These results serve as a basis for the validation of the FEM simulation model in terms of lateral blade displacement. The comparison of the measurements during the cut and during the no-load period suggests that the lateral displacement of the blade is mainly caused by the process forces. The values of $u_{x,t}$ approximately range from −0.25 mm to 0.5 mm. At the cut-changeover area, this entails a step of the lateral edge shape of approximately 0.75 mm. In essence, the blade shears at the cut-end about 0.75 mm deeper into the plate (along the x-direction) than at the start of cut. This blade motion is fully inline with the typical

Post-print version of the article: A. Zeiler, A. Steinboeck, A. Kugi, and M. Jochum, "Lateral forces in rolling-cut shearing and their consequences on common edge defects," *Journal of Manufacturing Science and Engineering*, vol. 141, no. 4, 41001-1–41001-9, 2019. DOI: 10.1115/1.4042578
The content of this post-print version is identical to the published paper but without the publisher's final layout or copy editing.

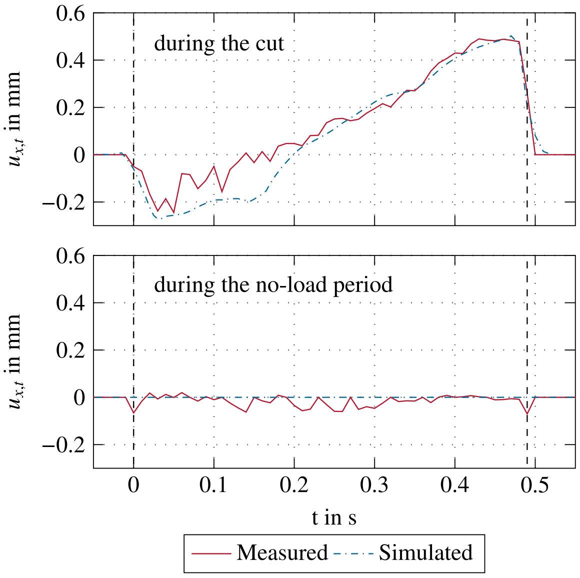

Fig. 7 Measured and simulated lateral displacement of the upper blade at the shearing point

sawtooth-shaped edges, which are outlined in Fig. 4. Figure 8 shows this longitudinal edge shape measured according to Sec. 4 and the measured lateral blade displacement.

The similarity of these measurements clearly corroborates the hypothesis that the varying lateral displacement of the blade causes the nonuniform edge shape of the plate. The sawtooth-like edge shape occurs more or less for all heavy plates with a thickness above 25 mm. Generally, the amplitude of the sawtooth shape increases with the plate thickness and reaches values up to 1.5 mm for heavy plates with a thickness of 42 mm. Note that the longitudinal edge shape was manually measured at discrete points along the z-direction. These spatial coordinate values are transformed into the time domain (by inversion of $z_s(t)$) to make them compatible with the abscissa of Fig. 8.

Clearly, the clearance between the upper and the lower blade changes upon any relative lateral displacement between these two blades. Temporarily installed laser sensors showed that the lateral displacement of the machine frame including the lower blade is negligibly small. Therefore, the clearance corresponds nearly directly with the lateral upper blade motion and various clearance values occur at different shearing points z_s. For the experiment, a nominal clearance of $C_{nom} = 2.6$ mm was adjusted under no-load conditions. So the peak–peak lateral displacement value 0.75 mm of the upper blade causes a 29 % change of the clearance. As pointed out by Sauer [18], the fracture behavior and the edge quality depend significantly on the clearance. Hence, different values of the effective clearance at different shearing points z_s lead to variations of the edge quality even in the area between the cut-changeovers.

5.2 Forces. Figure 9 shows the simulated lateral force $F_x(t)$ acting on the upper blade. This simulation result was obtained from the FEM model with a fully constrained upper blade as described in Sec. 2. The black dashed lines mark the start and end of the rolling-cut. F_x is the sum of contact forces between the plate and the blade. Generally, the majority of the contact forces acts in and around the region of the shear zone, as illustrated in Fig. 9.

The lateral force shows a similar behavior as the lateral blade motion. At the beginning of the cut ($t = t_1$), F_x pushes the upper blade outward, i.e., away from the plate center. During the cut, F_x changes its sign and then increasingly pulls the upper blade toward the plate center ($t = t_2$ and $t = t_3$). This is an interesting phenomenon because $F_x < 0$ is usually assumed in the literature. This raises the question why F_x varies so much and changes its sign. This will be addressed in Sec. 6.

Another interesting quantity in RCS is the cutting force $F_y(t)$ acting on the upper blade in the y-direction. Because F_y is clearly the highest force that appears during the RCS process, it is crucial for machine design. In this work, F_y is used as an additional means of validating the FEM model based on force models published in the literature. In Fig. 10, the simulated cutting force F_y is shown by the solid line. F_y shows an initial overshoot (cut starts) and then gradually decreases.

This gradual decrease is mainly caused by a variation of the shearing angle $\alpha_s(t)$, which is shown in Fig. 11. As described in Sec. 1, the shearing angle depends on the drive-kinematics and the plate thickness. Hence, this variation indicates the suboptimal design of the drive-kinematics. The relation between the cutting force F_y and the shearing angle α_s is usually described as indirectly proportional in the literature (see, for instance, Ref. [18] or [19]). Considering Figs. 10 and 11, this relation is obvious.

In Ref. [20], this behavior is demonstrated by measurements for guillotine-shearing. The author of Ref. [11] presents a semi-empirical formula for the steady-state cutting force F_y in guillotine-shearing (straight upper and lower blades) and validated it by numerous experiments. Sauer's formula considers the shearing angle, material parameters, and cutting geometry. The formula is

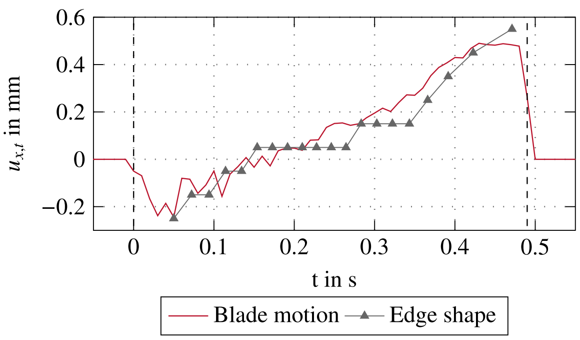

Fig. 8 Comparison of measured longitudinal edge shape and measured lateral upper blade motion

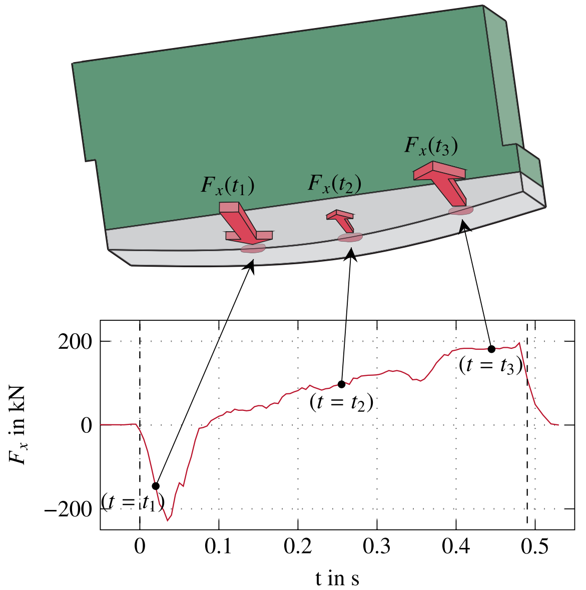

Fig. 9 Simulated lateral cutting force acting on the upper blade

Post-print version of the article: A. Zeiler, A. Steinboeck, A. Kugi, and M. Jochum, "Lateral forces in rolling-cut shearing and their consequences on common edge defects," *Journal of Manufacturing Science and Engineering*, vol. 141, no. 4, 41001-1–41001-9, 2019. DOI: 10.1115/1.4042578
The content of this post-print version is identical to the published paper but without the publisher's final layout or copy editing.

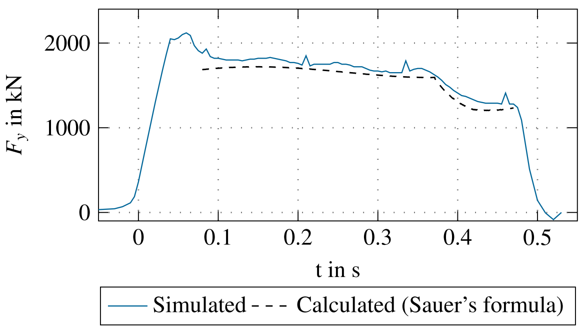

Fig. 10 Simulated and semi-empirically calculated cutting force F_y

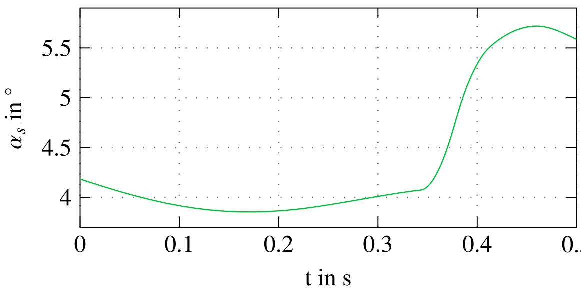

Fig. 11 Shearing angle $\alpha_s(t)$ for a plate thickness of 30 mm

summarized in Appendix. Based on the pre-calculated shearing angle α_s, Sauer's formula for the cutting force yields the black dashed line shown in Fig. 9. The formula is only valid for steady-state operation and consequently plotted just for these time intervals. The good agreement between the calculated and the simulated cutting force also corroborates the validity of the simulation model.

6 Discussion of the Varying Lateral Force

In this section, the following questions will be answered:

- What are the reasons for the variation of the lateral force?
- Does the design of the drive-kinematics influence the lateral force?

The major forces between the upper blade and the plate act in the relevant contact area around the shearing point z_s. This area on the plate is illustrated in Fig. 12(*a*). In case of high lateral displacement of the upper blade toward the center of the plate, there could occur additional contact forces between the trimmed side surface of the plate and the side surface of the upper blade. Compared with the forces in the relevant contact area, these additional forces are rather small. Figures 12(*b*) and 12(*c*) show two sectional views in the *xy*-plane of the shearing process at points z_{ip1} and z_{ip2} at the same time. Both points are located in the relevant contact area at the considered time. The intersection plane at z_{ip1} is located close to the tip of the cut, where the upper blade just slightly penetrates the plate. The intersection plane at z_{ip2} is located just before the material fracture, i.e., just before the shearing point. For all forces per unit length shown in Fig. 12, the short notation $\tilde{F}_i = F_i(t, z_{ip})$ is used. By analogy $\tilde{u}_{sc} = u_{sc}(t, z_{ip})$ and $\tilde{v}_b = v_b(t, z_{ip})$ refer to the corresponding displacements and velocities, respectively. The total process force acting on the upper blade is consequently defined as

$$F_i(t) = \int_{z_0}^{z_1} \tilde{F}_i(t)\, \mathrm{d}z, \qquad i \in \{x, y\} \tag{5}$$

where z_0 and z_1 denote the first and the last points of contact between the plate and the upper blade along the *z*-coordinate. Forces are generally defined in consistent directions in this paper. The forces in Fig. 12 constitute an exception because they are illustrated in their effective direction to enhance clarity. The vertical force component $\tilde{F}_y$ consists of a dominant normal component $\tilde{F}_{y,n}$ at the bottom surface of the blade and a smaller shearing force (frictional force) $\tilde{F}_{y,f}$ at the side surface of the blade. These forces act as distributed loads and have their point of origin close to the cutting edges [21]. The force $\tilde{F}_{y,n}$ causes plastic deformation and contributes to the (vertical) bending displacement $\tilde{u}_{sc}$ along the lateral coordinate *x*. However, the actual bending displacement of the scrap along the lateral direction is a complex function of the 3D stress field, plastic deformation state, and boundary conditions of the whole scrap volume. These boundary conditions include a Dirichlet boundary condition at the lower scrap knife (see Fig. 1). As indicated in Fig. 12, the bending displacement of the scrap along the lateral direction causes a lateral shearing force component $\tilde{F}_{x,f}$ on the bottom surface of the upper blade. This frictional shearing force (frictional force) due to the bending displacement along the lateral direction was investigated by Romanowski [22] in the context of blanking. Depending on the sign of $\tilde{u}_{sc}$, the shearing component $\tilde{F}_{x,f}$ points either along the positive or negative

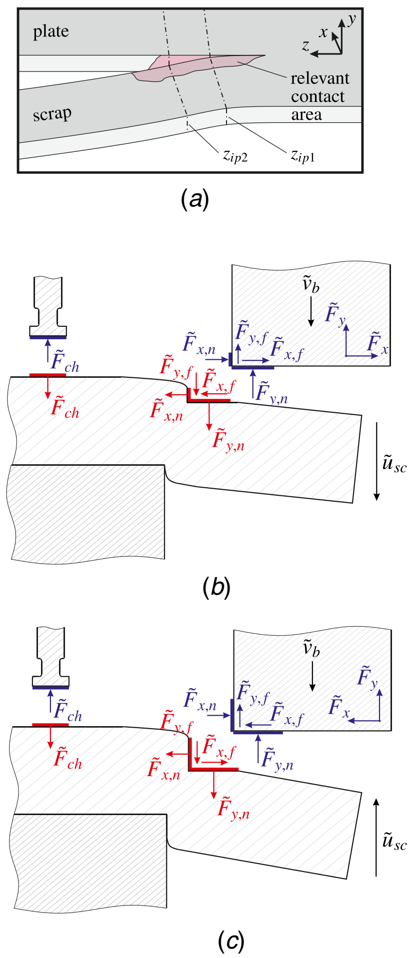

Fig. 12 Velocities, displacements, and forces per unit acting on the blade, the blank holder, and the plate: (*a*) plate with illustrated relevant contact area and sectional planes at z_{ip1} and z_{ip2}, (*b*) sectional plane at z_{ip1}, and (c) sectional plane at z_{ip2}

Post-print version of the article: A. Zeiler, A. Steinboeck, A. Kugi, and M. Jochum, "Lateral forces in rolling-cut shearing and their consequences on common edge defects," *Journal of Manufacturing Science and Engineering*, vol. 141, no. 4, 41001-1–41001-9, 2019. DOI: 10.1115/1.4042578
The content of this post-print version is identical to the published paper but without the publisher's final layout or copy editing.

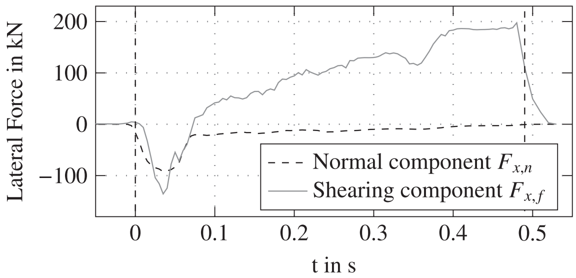

Fig. 13 Simulated normal and shearing component of the lateral force on the upper blade

x-direction. Similar to the vertical force on the upper blade, the lateral force $\tilde{F}_x$ consists of the mentioned shearing component $\tilde{F}_{x,f}$ at the bottom surface of the blade and a normal compressive component $\tilde{F}_{x,n}$ at the side surface of the blade. The simulated forces $F_{x,f}$ and $F_{x,n}$ are shown in Fig. 13. The compressive force $F_{x,n}$ is rather small and significant nonzero values occur only at the beginning of the cut, i.e., until the first material fracture occurs. The dominating part is clearly the shearing component $F_{x,f}$. This component also causes a sign change of F_x. In the region of the intersection plane at z_{ip1}, the bending displacement $\tilde{u}_{sc}$ occurs certainly in a mathematically negative sense (clockwise) due to the high translational velocity $\tilde{v}_b$ of the upper blade. Hence, the shearing force component $\tilde{F}_{x,f}$ points along the negative x-direction (see Fig. 12(*a*)). However, in the region of the intersection plane at z_{ip2}, the complex plastic deformation state and the stress field yield an upward bending displacement (counterclockwise $\tilde{u}_{sc}$) of the scrap, which evokes a positive force $\tilde{F}_{x,f}$ (see Fig. 12(*b*)). Hence, at each time the lateral shearing force $F_{x,f}$ is the sum of negative contact shearing forces $\tilde{F}_{x,f}$ in the region of the tip of the cut and positive contact shearing forces $\tilde{F}_{x,f}$ in the region of the shearing point (fracture of the plate). Likewise the FEM simulation shows this behavior. As $F_{x,f}$ grows within the cut, the region where the bending displacement along the lateral direction points upward grows as well.

The question arises, if this is induced by the varying impact of the drive-kinematics. At least, this is indicated due to the variation of the shearing angle $\alpha_s(t)$ (see Fig. 11). To figure out if a pure rolling-cut would lead to a constant lateral force F_x, an FEM simulation with an 18-m diameter full-circle disc blade is carried out. The disc blade rolls and cuts with a constant velocity along the z-direction. Clearly, such a giant blade is suitable for theoretical investigations only. Figure 14 shows the simulated lateral force on the upper blade for a full-circle disc blade and the considered rolling-cut shear system both with and without a scrap knife. The figure shows that trimming with the large diameter full-circle disc blade yields a practically constant lateral force. Small variations appear only at the beginning of the cut and due to negligible numerical inaccuracies. This result demonstrates that the variation of the lateral force can be reduced by adapting the drive-kinematics. Because the varying lateral force is the main reason for the lateral displacement of the upper blade (changing clearance) and thus the quality defects described in Sec. 1, an optimization of the drive-kinematics is expected to improve the quality of the sheared edges. The work of Ma et al. [7] corroborates this potential. They redesigned the whole drive-kinematics including the connecting rods, crankshafts, and blade carrier with the objective to imitate a pure rolling-cut. The sheared edges were observed to have a higher quality. However, the work of Ma et al. [7] does neither explain the reason for the observed improvement nor does it motivate why the pure rolling-cut was aimed for.

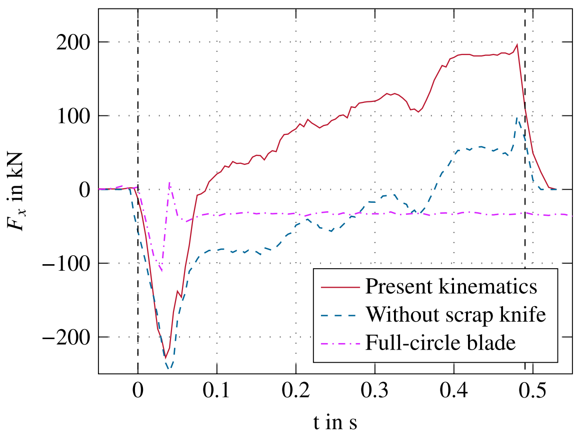

Fig. 14 Simulated lateral force on the blade when using the present kinematics, the present kinematics without scrap knife, and the full-circle disc blade

To investigate the connection between the drive-kinematics of the considered industrial rolling-cut shear and the corresponding lateral force F_x, shown in Fig. 14 by the solid line, a single cut is partitioned into three intervals:

Interval I: This interval represents the beginning of the cut. During this interval, the upper blade of the considered industrial rolling-cut shear undergoes mainly a vertical translation (defined by the present drive-kinematics). Such a vertical translation is similar to the blanking process, which explains why the lateral force in RCS during interval I shown in Fig. 14 is similar to the lateral force in the blanking process (see Ref. [23]) before material fractures. The vertical cutting force F_y (see Fig. 10) grows linearly until the plastic deformation of the plate starts. This cutting force induces consequently a downwards bending displacement along the lateral direction as illustrated in Fig. 12(*a*). Due to the mainly vertical downwards translation of the upper blade, an upwards bending displacement along the lateral direction (see Fig. 12(*a*)) is unlikely and $\tilde{F}_{x,f}$ points along the negative x-direction in most regions of the relevant contact area. Consequently, F_x is negative in this interval.

This behavior is observable with the full-circle disc blade as well. The amplitude of the negative force is smaller in this case, because the full-circle disc performs a purely longitudinal motion (in the direction z) in the simulation.

Interval II: During this interval, the scrap from the previous cut that is already separated, but not separated by the scrap knife, plays an important role. As shown in Fig. 1, this part of the scrap cannot freely bend downward because of the lower scrap knife. To demonstrate the consequences of this restricted bending motion of the scrap on the lateral force acting on the upper blade, Fig. 14 shows simulation results for the RCS process with and without the scrap knife. During this interval, the motion of the upper blade is very similar to that of the full-circle disc shear. This explains the similarity of the lateral force shown in Fig. 14 for the RCS process without scrap knife and the full-circle disc blade during interval II. In contrast, the lateral force significantly increases for the rolling-cut shear configuration with scrap knife (configuration as in the considered industrial plant). These results indicate that the position of the scrap knife influences the lateral force F_x and hence also the edge quality.

Interval III: For the rolling-cut shear configuration, the lateral force F_x increases during interval III. This force grows significantly after time $t = 0.35$ s. Considering the shearing angle $\alpha_s(t)$ shown in Fig. 11, it is recognizable that this quantity also increases significantly after $t = 0.35$ s. The increase of α_s yields an increasing curvature of the scrap along the longitudinal coordinate z. In order to outline the curvature of the scrap in the longitudinal direction, the vertical displacement $u_y(t, x_d, z)$

Post-print version of the article: A. Zeiler, A. Steinboeck, A. Kugi, and M. Jochum, "Lateral forces in rolling-cut shearing and their consequences on common edge defects," *Journal of Manufacturing Science and Engineering*, vol. 141, no. 4, 41001-1–41001-9, 2019. DOI: 10.1115/1.4042578
The content of this post-print version is identical to the published paper but without the publisher's final layout or copy editing.

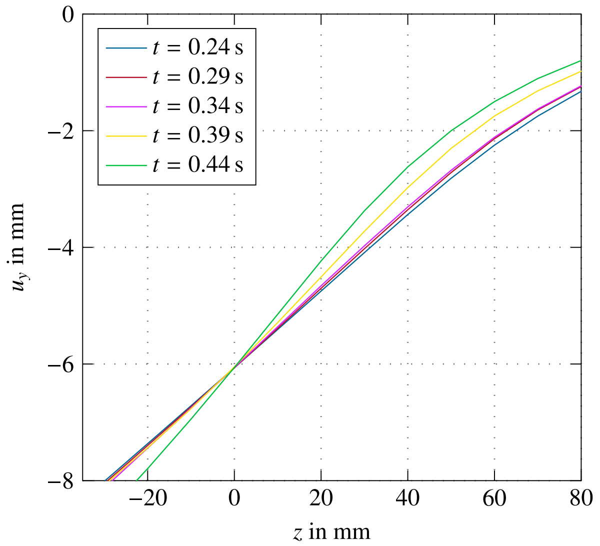

Fig. 15 Vertical displacement of the scrap along the longitudinal *z*-direction

of the scrap calculated in the FEM simulation is shown in Fig. 15. This displacement is measured in a plane parallel to the yz-plane and $x_d = 10$ mm outside of the cut. The displacement is plotted depending on the relative coordinate z with an offset to ensure $u_y(t, x_d, 0) = -6$ mm to enhance comparability. It can be seen that the curvature of the scrap in the longitudinal direction increases progressively during the cut. This progressive increase is very similar to the lateral force F_x and obviously the shearing angle $\alpha_s(t)$. It is a well-known effect that the curvature of shell-like structures in one direction (in this case the z-direction) induces a spatial increasing of the shell stiffness (i.e., the bending stiffness along the lateral x-direction). Hence, the bending displacement $\tilde{u}_{sc}$ tends to point in the positive y-direction (upwards). Consequently, the region in the relevant contact area, where an upward bending displacement $\tilde{u}_{sc}$ occurs (see Fig. 12(b)), expands. Hence, the relevant contact area, where positive contact shearing forces $\tilde{F}_{x,f}$ act, expands as well. The bending displacements $\tilde{u}_{sc}(t, x, z_P)$ along the x-direction are shown in Fig. 16 to corroborate the progressive upward bending displacement.

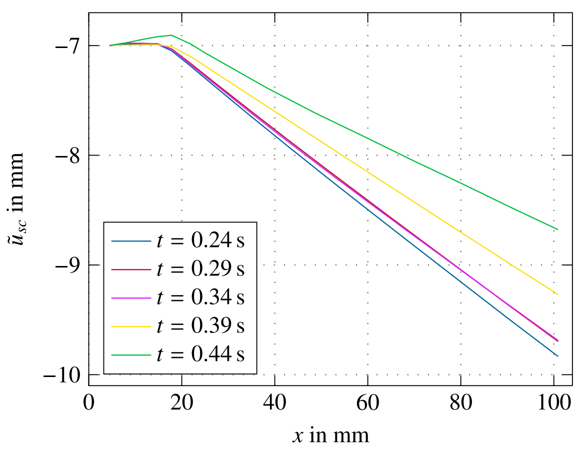

Fig. 16 Vertical bending displacement of the scrap along the lateral direction (x-direction)

A comparison between the shearing angle α_s shown in Fig. 11, the curvature of the scrap in longitudinal direction shown in Fig. 15, the bending displacement of the scrap in the lateral direction shown in Fig. 16, and the simulated lateral force for the rolling-cut shear configuration shown in Fig. 14 reveal that all these quantities correlate positively. In particular, the significant change of all these quantities between $t = 0.39$ s and $t = 0.44$ s is obvious. In contrast, these quantities are rather constant between $t = 0.29$ s and $t = 0.34$ s.

The results presented in this section indicate the significant influence of the design of the drive-kinematics and the position of the scrap knife on the lateral force. Furthermore, it was shown in simulations that the full-circle disc blade is optimal in the sense that the lateral force on this blade is practically constant. The differences between the industrial rolling-cut shear under consideration and the ideal full-circle disc blade in terms of displacements and process forces were discussed. An important conclusion from the conducted analysis is that the variation of the curvature of the scrap in the longitudinal direction causes varying lateral process forces and thus varying lateral displacements of the upper blade.

7 Conclusions and Outlook

In the present work, the lateral process forces in rolling-cut shears of heavy plates were investigated. The variation of the lateral process force on the upper blade was identified as the root cause for an unintended lateral motion of the upper blade, an unintended varying clearance, and thus commonly observed quality defects of the sheared edges. To analyze the RCS process, an FEM model was developed and in situ measurements of the lateral motion of the upper blade of an industrial rolling-cut shear were conducted. The simulated and the measured lateral blade motions show good agreement. Moreover, the longitudinal shape of the sheared edge was measured and shown to coincide with the lateral displacement of the upper blade. Based on the FEM model and the measurement results, a physical explanation of the variation of the lateral force was given. A significant influence of the drive-kinematics of the upper blade on the variation of lateral force was observed. Future research could utilize the obtained deep understanding of the rolling-cut process to optimize the drive-kinematics as well as the plant geometry. The objective of such an optimization would be a constant lateral process force and consequently a constant clearance during each cut. This would reduce or even avoid common quality defects of the sheared edge.

Appendix: Sauer's Formula for the Cutting Force

The author of Ref. [11] computes the cutting force (vertical process force) in the following form:

$$F_y = F_y^c + F_y^b \tag{A1}$$

where F_y^c denotes the force needed for the fracture of the material and F_y^b denotes the force needed for bending the scrap in the longitudinal direction. F_y^c was specified by Zelikow [20] in the following form:

$$F_y^c = 0.6\varepsilon_s\sigma_m t_p^2 \frac{1}{\tan(\alpha_s)} \tag{A2}$$

In this equation, t_p denotes the sheet thickness, σ_m the tensile strength, and ε_s the vertical penetration of the upper blade until fracture occurs. The parameter ε_s is determined based on visual inspection of the sheared edge and chosen as $\varepsilon_s = 0.28$. The shearing angle α_s, which depends on the drive-kinematics and the plate thickness, is shown in Fig. 11 for the considered rolling-cut shear. In guillotine-shearing, this value is generally constant. In case of the considered rolling-cut shear, α_s varies obviously due to the suboptimal drive-

Post-print version of the article: A. Zeiler, A. Steinboeck, A. Kugi, and M. Jochum, "Lateral forces in rolling-cut shearing and their consequences on common edge defects," *Journal of Manufacturing Science and Engineering*, vol. 141, no. 4, 41001-1–41001–9, 2019. DOI: 10.1115/1.4042578
The content of this post-print version is identical to the published paper but without the publisher's final layout or copy editing.

kinematics. The force needed for bending the scrap in the longitudinal direction was specified by Sauer [11] and is given by

$$F_y^b = \frac{3}{8}\sigma_y^0 t_p w_{sc}\ \tan(\alpha_s)\frac{1}{\varepsilon_s} \tag{A3}$$

where w_{sc} describes the scrap width.

References

[1] Ghozzi, Y., Labergere, C., and Saanouni, K., 2014, "Modelling and Numerical Simulation of Thick Sheet Double Slitting Process Using Continuum Damage Mechanics," Int. J. Damage Mech., **23**(8), pp. 1150–1167.

[2] Biao, L., Yali, M., Delun, W., and Shaoping, B., 2017, "Kinematic Design of a Seven-Bar Linkage With Optimized Centrodes for Pure-Rolling Cutting," Hindawi Math. Problems Eng. **2017**, p. 11.

[3] Wick, C., Benedict, J. T., and Veilleux, R. F., 1984, "Forming," *Tool and Manufacturing Engineers Handbook*, 4 ed, Vol. 2, Society of Manufacturing Engineers, Dearborn, MI.

[4] Murakawa, M., and Lu, Y., 1997, "Precision Cutting of Sheets by Means of a New Shear Based on Rolling Motion," J. Mater. Process. Technol., **66**, pp. 232–239.

[5] Ma, L.-F., Huang, Q.-X., and Chu, Z.-B., 2012, "Establishment of Optimal Blade Clearance of Stainless Steel Rolling-Cut Shear and Test of Shearing Force Parameters," J. Iron Steel Res. Int., **19**(9), pp. 52–61.

[6] Zyryanov, V., Ivanov, A., and Gaitanov, I., 2004, "Use of Shears With a "Rolling Cut"," Metallurgist, **48**(3), pp. 51–52.

[7] Ma, L.-F., Huang, Q.-X., and Wang, J.-M., 2007, "Mechanical Properties of New Type Negative Offset Structure During Shearing Process of Heavy Steel Plate," J. Iron Steel Res. Int., **14**(5), pp. 31–35.

[8] Nothhaft, K., 2014, "Scherschneiden Höchstfester Blechwerkstoffe im Offenen Schnitt." PhD Thesis, Technical University of Munich.

[9] Guo, Y., and Dornfeld, D., 2000, "Finite Element Modeling of Burr Formation Process in Drilling 304 Stainless Steel," J. Manuf. Sci. Eng., **122**, pp. 612–619.

[10] Rao, S., 2011, *The Finite Element Method in Engineering*, Vol. 5, Elsevier, Amsterdam.

[11] Sauer, R., 1980, "Untersuchung Zur Mechanik des Kaltscherens," Ph.D. thesis, RWTH Aachen.

[12] Trzepiecinski, T., Bazan, A., and Lemu, H., 2015, "Frictional Characteristics of Steel Sheets Used in Automotive Industry," Int. J. Automot. Technol., **16**(5), pp. 849–863.

[13] Lemiale, V., Chambert, J., and Picart, P., 2009, "Description of Numerical Techniques with the Aim of Predicting the Sheet Metal Blanking Process by FEM Simulation," J. Mater. Process. Technol., **209**, pp. 2723–2734.

[14] Wang, K., 2016, "Calibration of the Johnson-Cook Failure Parameters as the Chip Separation Criterion in the Modelling of the Orthogonal Metal Cutting Process," Master's thesis, McMasters University, Hamilton, Canada.

[15] Johnson, G., and Cook, W., 1985, "Fracture Characteristics of Three Metals Subjected to Various Strains, Strain Rates, Temperatures and Pressures," Eng. Fract. Mech., **21**(1), pp. 31–48.

[16] Wierzbicki, T., Bao, Y., and Lee, Y., 2005, "Calibration and Evaluation of Seven Fracture Models," Int. J. Mech. Sci., **47**, pp. 719–743.

[17] Bacha, A., Daniel, D., and Klocker, H., 2008, "Metal Ductility at Low Stress Triaxiality Application to Sheet Trimming," J. Mater. Process. Technol., **203**, pp. 480–497.

[18] Sauer, R., 1979, *Atlas für das Kaltscheren*. Max-Planck-Institut für Eisenforschung and Verein Deutscher Eisenhüttenleute, Düsseldorf.

[19] Atkins, T., 2009, *The Science and Engineering of Cutting – The Mechanics and Processes of Separating, Scratching and Puncturing Biomaterials, Metals and Non-Metals*, 1st ed. Butterworth-Heinemann, London.

[20] Zelikow, A., 1954, *Hilfsmaschinen der Walzstraßen*, VEB Verlag Technik, Berlin.

[21] Yamasaki, S., and Ozaki, T., 1991, "Shearing of Inclined Sheet Metals," Japan Soc. Mech. Eng. Int. J., **34**(4), pp. 533–539.

[22] Romanowski, W., 1979, *Spravochnik po holodnoj shtampovke*, 6 ed. Leningradskoe otdelenie (Leningrad "Maschinenbau").

[23] Kopp, T., Stahl, J., and Demmel, P., 2016, "Experimental Investigation of the Lateral Forces During Shear Cutting With an Open Cutting Line," J. Mater. Process. Technol., **238**, pp. 49–54.

Post-print version of the article: A. Zeiler, A. Steinboeck, A. Kugi, and M. Jochum, "Lateral forces in rolling-cut shearing and their consequences on common edge defects," *Journal of Manufacturing Science and Engineering*, vol. 141, no. 4, 41001-1–41001-9, 2019. DOI: 10.1115/1.4042578